JOURNAL OF VIROLOGY, May 2009, p. 4275–4286 Vol. 83, No. 9
0022-538X/09/$08.00+0 doi:10.1128/JVI.02383-08

Replicon Particles of Venezuelan Equine Encephalitis Virus as a Reductionist Murine Model for Encephalitis▽

Alexandra Schäfer,* Alan C. Whitmore, Jennifer L. Konopka,† and Robert E. Johnston

Department of Microbiology and Immunology, Carolina Vaccine Institute, The University of North Carolina at Chapel Hill, Chapel Hill, North Carolina 27599

Received 17 November 2008/Accepted 5 February 2009

Venezuelan equine encephalitis virus (VEE) replicon particles (VRP) were used to model the initial phase of VEE-induced encephalitis in the mouse brain. VRP can target and infect cells as VEE, but VRP do not propagate beyond the first infected cell due to the absence of the structural genes. Direct intracranial inoculation of VRP into mice induced acute encephalitis with signs similar to the neuronal phase of wild-type VEE infection and other models of virus-induced encephalitis. Using the previously established VRP-mRNP tagging system, a new method to distinguish the host responses in infected cells from those in uninfected bystander cell populations, we detected a robust and rapid innate immune response in the central nervous system (CNS) by infected neurons and uninfected bystander cells. Moreover, this innate immune response in the CNS compromised blood-brain barrier integrity, created an inflammatory response, and directed an adaptive immune response characterized by proliferation and activation of microglia cells and infiltration of inflammatory monocytes, in addition to $CD4^+$ and $CD8^+$ T lymphocytes. Taken together, these data suggest that a naïve CNS has an intrinsic potential to induce an innate immune response that could be crucial to the outcome of the infection by determining the composition and dynamics of the adaptive immune response. Furthermore, these results establish a model for neurotropic virus infection to identify host and viral factors that contribute to invasion of the brain, the mechanism(s) whereby the adaptive immune response can clear the infection, and the role of the host innate response in these processes.

Virus infections of the central nervous system (CNS) can have fatal consequences, and the ability of the CNS to establish an adequate innate immune response to a pathogen is essential for a positive outcome (24). The CNS has historically been considered an "immunologically privileged" site based on the following observations. First, to minimize the occurrence of autoimmunity, the CNS lacks a lymphatic system that captures potential CNS antigens. Second, the expression of class I and II major histocompatibility complex (MHC) molecules, which are critical for antigen presentation, is extremely low and highly regulated in neurons and in the CNS in general (9, 36). Brain-residing microglia cells are the only cells that express MHC class II molecules but show a limited capacity for antigen presentation to naïve T cells, even when activated, and no brain-residing population of dendritic cells (DCs) has been identified (16, 52). Finally, the blood-brain barrier (BBB) imposes a complex barrier to cell extravasation from circulating blood (25, 44). However, the "immune privilege" can be completely lost after an infection or inflammation is established in the CNS. Evidence of this includes activation of brain-residing microglia cells, expression of proinflammatory cytokines and chemokines, breakdown of the BBB and resulting influx of DCs and inflammatory leukocytes, and drainage of antigen. The cellular infiltration into the brain in response to inflammation, infection, and injury is weaker and slower than inflammation in peripheral tissues. Even so, the brain's innate immune and proinflammatory responses can be induced rapidly (3, 25, 35, 37).

The early events in the antiviral immune response in the CNS play an important role in the development of disease, pathology, and clearance of the infecting virus. The consequence of a virus infection in the CNS is dependent upon viral cell tropism, the ability of the virus to spread, and the characteristics of the immune response to the infection. An inappropriate immune response to virus infection of the CNS can cause severe encephalitis, leading to significant neuropathology or even death of the host. In these situations, it has been difficult to determine whether disease pathogenesis is predominantly caused by the virus itself or by the immune response (6, 24, 48).

Venezuelan equine encephalitis virus (VEE) is a mosquito-borne alphavirus associated with periodic epidemics and equine epizootics in the western hemisphere (23). In horses, rodents, and humans, infection with VEE induces a wide spectrum of disease, ranging from an asymptomatic infection to lethal encephalitis. Clinical signs, which usually appear 2 to 5 days after infection, are characterized by fever, depression, and anorexia. The progression to encephalitis and death correlates with the magnitude of viremia (60). While enzootic strains cause little to no clinical illness, disease induced by epizootic strains can be severe, with a high mortality rate in rodents and horses (57). Death is rare in humans (1 to 2%), but neurological symptoms appear in 5 to 15% of cases (60).

A peripheral subcutaneous infection of mice leads to biphasic disease: an initial peripheral phase within 1 to 2 days postinoculation, in which the virus replicates mainly in lymphoid

* Corresponding author. Mailing address: Carolina Vaccine Institute, The University of North Carolina at Chapel Hill, Chapel Hill, NC 27599. Phone: (919) 966-4026. Fax: (919) 843-6924. E-mail: aschaefe@email.unc.edu.

† Present address: Lamb Center for Pediatric Research, Vanderbilt University Medical Center, Nashville, TN 37232.

▽ Published ahead of print on 18 February 2009.

and myeloid tissues (the "lymphotropic" phase), followed by a neurotropic phase (20). The initial lymphotropic phase is characterized by the development of a high-titer serum viremia. This is followed by clearance of the virus from the periphery 3 to 4 days postinoculation. CNS invasion initiates the neurotropic phase of the disease. Neuroinvasion is thought to occur via the olfactory neuroepithelium, occurs 2 to 3 days after inoculation, and leads to the death of the animal by 6 to 7 days after infection (5, 10, 21, 47, 56).

Further study of the neurotropic phase of VEE infection has been hampered by the destructive consequences of the wild-type virus. Wild-type virus spreads throughout the brain, and animals die within 6 to 7 days after infection (27). Further, the virus causes severe deterioration of the brain tissue, making it difficult to decipher the host responses in infected cells and signaling to uninfected bystander cells (29). To examine the earliest stages of VEE neuropathogenesis, we used VEE replicon particles (VRP) to model the onset of the infection.

VRP are propagation-defective particles which contain a VEE-derived genome, based on the infectious cDNA clone. The VRP genome is modified so that the structural genes are deleted and replaced by a heterologous gene of interest. To facilitate assembly of VRP, two helper RNAs that include the capsid and glycoprotein genes but lack a packaging signal are supplied in *trans*. When VRP infect cells, they undergo only one round of infection, during which the VRP genome replicates and the heterologous gene is expressed at high levels (42). Recently, Konopka et al. (29) have used VRP expressing a FLAG-tagged poly(A)-binding protein (FLAG-PABP) to infect mice. In this instance, only the initially infected and replicating cells expressed FLAG-PABP, and this molecule formed RNPs with cellular messages in the infected cells only. Subsequent immunoprecipitation of RNPs derived from the affected tissue with anti-FLAG antibodies preferentially allowed analysis of cellular transcriptional activity in the infected cell population, while immunoprecipitation with anti-PABP yielded the mRNP population from both infected and uninfected cells. Konopka et al. (29) used the mRNP tagging system to define a two-step innate immune response whereby activation of host genes within infected cells leads to activation of bystander cells. VRP expressing marker proteins or the VRP-mRNP tagging system are powerful tools for the study of the earliest events in VEE neuropathogenesis in the mouse.

In this report, we describe an in vivo model of alphavirus-induced acute encephalitis. Following intracranial (i.c.) inoculation of VRP, the naïve CNS mounted a rapid and robust innate immune response. The BBB was compromised, cells of the adaptive immune response entered the brain from the periphery, and the VRP infection was successfully cleared from the brain.

MATERIALS AND METHODS

Animals, VRP production, and infections. Female BALB/c mice were purchased from Charles River and used at 4 to 8 weeks of age. After mice were treated with a ketamine-xylazine mixture, they were inoculated i.c. or in the left rear footpad with 2×10^6 IU of FLAG-PABP VRP, a VRP which expresses a FLAG-PABP fusion protein under the control of the VEE 26S promoter (29), in VRP diluent (endotoxin-free phosphate-buffered saline [PBS] supplemented with 1% donor calf serum; total volume, 10 μl). For immunohistochemistry studies, mice were inoculated with VRP expressing enhanced green fluorescence protein under the control of the 26S promoter (eGFP-VRP). Mock-treated animals were inoculated with 10 μl diluent alone. After inoculation with VRP, mice were monitored for disease signs and weighed at 24-h intervals. All of the replicon particles used in this study were packaged in the wild-type VEE (V3000) envelope (42). For assembly, appropriate replicon RNA and helper RNAs were electroporated into BHK-21 cells. After confirming the absence of propagating recombinant virus by passage in BHK-21cells, VRP preparations were concentrated by centrifugation and titers were determined.

Evaluation of BBB permeability. Mice were inoculated in the footpad or i.c. with 2×10^6 IU FLAG-PABP VRP, null VRP (VRP without an inserted heterologous gene), or UV-inactivated FLAG-PABP VRP. Intraperitoneal (i.p.) injection of 50 μg poly(I:C) in 50 μl 1× PBS served as a positive control. At 1, 2, and 4 days postinfection (dpi), mice were injected i.p. with 800 μl of 1% Evans blue dye in 1× PBS. One hour after Evans blue dye injection, mice were perfused with 2% paraformaldehyde (PFA) and their brains were harvested (59). To quantify Evans blue dye uptake, the harvested brains were weighed, snap-frozen in liquid nitrogen, and pulverized. The powder was washed in 1× PBS and then resuspended in 1 ml dimethyl sulfoxide. The samples were centrifuged at 13,000 × *g* for 10 min, the supernatants were removed, and the absorption at 611 nm was measured on a FLUOstar Omega microplate reader with the Omega software v1.02 (BMG Labtech) along with standards ranging from 0.3725 to 200 ng (58). The uptake of Evans blue dye was normalized for each brain sample (nanograms of Evans blue per milligram of brain homogenate) and analyzed in comparison to that of mock-infected animals.

Total RNA isolations and mRNP tag immunoprecipitation isolation. Total RNA was isolated from brain tissues of VRP-inoculated and mock-treated animals with a Qiagen Lipid Tissue Mini kit. VRP-infected cell RNA was isolated by the mRNP tagging method (29). At various time points postinfection with FLAG-PABP VRP, tissue lysates were prepared and divided and either anti-FLAG antibody- or anti-PABP antibody-coated agarose beads were added in excess to the lysate. The immunoprecipitate was dissociated by proteinase K digestion, and the RNA populations (from mRNP immunoprecipitated with either anti-FLAG or anti-PABP antibodies) were isolated by standard RNA extraction and precipitation (29).

Real-time PCR and analysis. Expression levels of different genes were measured by quantitative real-time PCR (RT-PCR) as previously described (29). Briefly, cDNAs were synthesized from mRNA by reverse transcription with oligo(dT); RT-PCR was then performed with TaqMan gene expression assays (Applied Biosystems) containing gene-specific primers and probes and an ABI Prism 7000 real-time PCR system. For analysis, all expression levels of target genes were normalized to that of the housekeeping gene *GAPDH* (ΔC_T). Gene expression values were then calculated based on the $\Delta\Delta C_T$ method, by using the mean of three untreated mice as the calibrator to which all other samples were compared. Relative expression levels were determined by using the following formula: Relative expression = $2^{\Delta\Delta}C^T$. For the analysis of mRNA tagging samples, two normalization steps were used to correct for (i) the disparity in the cell number in infected and mock-infected samples assayed by the mRNP tagging system and (ii) differences in immunoprecipitating antibody strength as described by Konopka et al. (29). The normalized C_T values then served as the input mock *GAPDH* value $2^{-(\Delta\Delta C_T)}$ for the standard ΔC_T analysis.

Isolation of mononuclear cells from the CNS and flow cytometry. Adult female BALB/c mice were anesthetized with a ketamine-xylazine anesthetic mixture and then inoculated i.c. with 2×10^6 IU FLAG-PABP VRP in a volume of 10 μl. Mock-treated animals were inoculated with 10 μl of diluent alone. At days 1, 2, 4, 7, 9, and 14 following infection, mice were euthanized and perfused with 1× PBS. Brains were then harvested, minced, and digested with collagenase (1.25 mg/ml) for 45 min at 37°C to isolate infiltrating cells. The cells were then passed through a 40-μm cell strainer, underlaid with 20% Percoll, and centrifuged for 20 min at 800 × *g* and 4°C. The pellet was resuspended in 30% Percoll, underlaid with 70% Percoll, and centrifuged for 20 min at 800 × *g* and 4°C. Banded cells were collected and washed twice with ice-cold 1× PBS. Live cells were counted by trypan blue exclusion. Mononuclear cells were then resuspended in fluorescence-activated cell sorter buffer (1× Hanks balanced salt solution, 1% fetal calf serum, 0.1% sodium azide) and stained with the following antibodies from eBioscience: fluorescein isothiocyanate-conjugated anti-CD3, phycoerythrin-conjugated anti-CD4, allophycocyanin-conjugated anti-CD8, fluorescein isothiocyanate-conjugated anti-CD11b, phycoerythrin-conjugated anti-CD11c, Pacific blue-conjugated anti-B220, biotin-conjugated anti-CD45 with a streptavidin-conjugated peridinin chlorophyll protein antibody, and allophycocyanin-conjugated anti-MHC class II. Donor species-matched antibodies conjugated with the appropriate fluorophore were used as isotype controls (eBioscience). Values for the CD45 isotype control account for approximately 10 to 15% of the $CD11b^+$ $CD11c^-$ cells in the positive gate. Seven-color fluorescence was assessed on a CyAn Fluorometer and analyzed with the Summit 2.1 software (33).

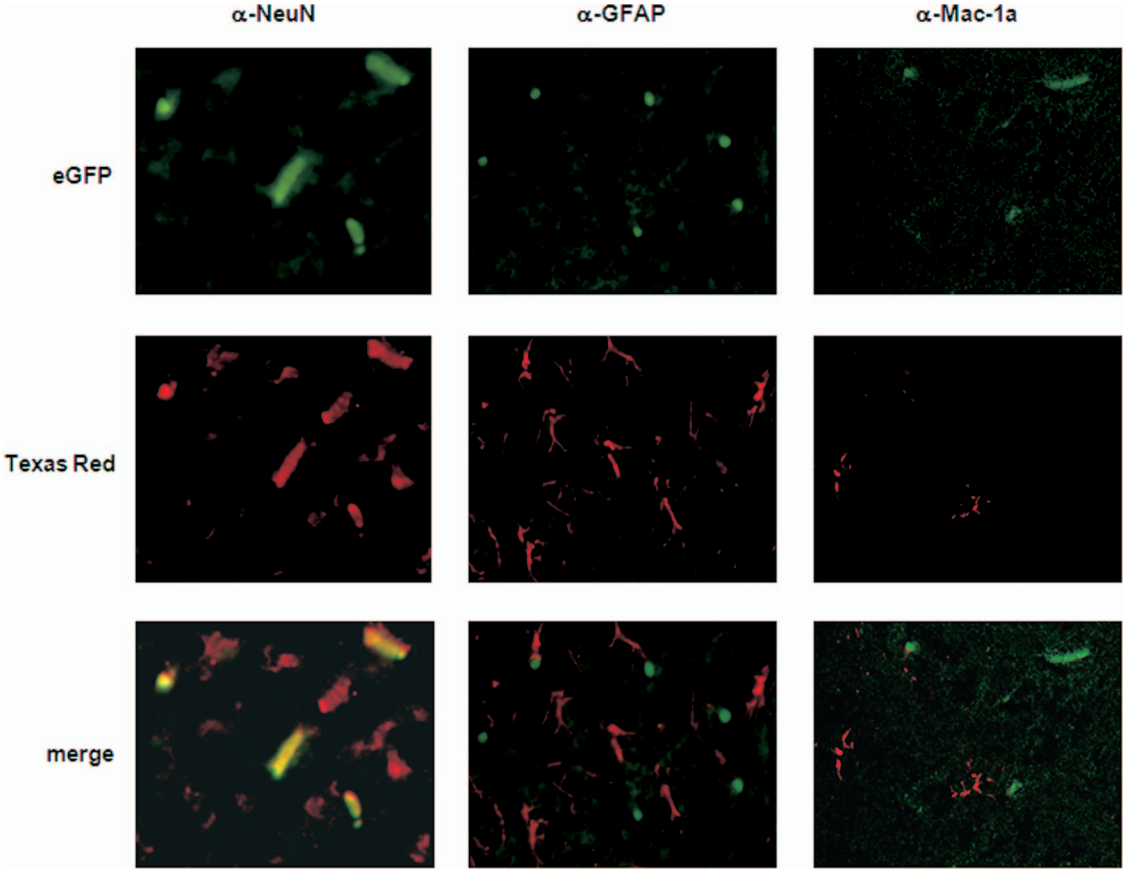

FIG. 1. VRP inoculated i.c. infect neurons. Adult female BALB/c mice were i.c. inoculated with 2×10^6 IU eGFP-VRP or with diluent alone as a mock-infected control. At day 1, 2 (shown here), or 4 postinfection, mice were euthanized and perfused with 2% PFA. Their brains were then cryoprotected and sectioned at 10 μm. Specific immunofluorescent staining (magnification, ×400) for neurons (α-NeuN; left panel), astrocytes (α-GFAP; middle panel), and microglia cells (α-Mac-1a; right panel) at the indicated time points is shown.

Immunohistochemistry. Mice were inoculated i.c. with VRP as described above. At days 1, 2, and 4 postinfection, inoculated mice were transcardially perfused with 2% PFA. Brains were removed and placed in 4% PFA overnight at 4°C. After rehydration in 30% sucrose solution for 24 h, brains were frozen in Tissue-Tek OCT Compound with a histobath and sectioned at 10 μm with a cryostat. Cryosections were mounted on poly-L-lysine-coated slides and air dried for 30 min at room temperature. Resident brain cell populations were then stained with anti-NeuN (neuronal nuclei, clone A60; Chemicon), anti-GFAP (glial fibrillary acidic protein, clone GA5; Chemicon), and anti-Mac-1a/CD11b (clone M1/70; eBioscience). Infiltrating cells were stained with anti-CD45 (clone 30-F11; BD Biosciences). After reaction with secondary antibodies (biotinylated anti-mouse and anti-rat immunoglobulin G; Vector) and the proper fluorophore-labeled avidin preparations, sections were examined with a Nikon FXA microscope.

RESULTS

Neurons are the principal target cells for VRP infection in the brain. Mice were infected i.c. with eGFP-VRP or with diluent alone as a negative control. The animals were sacrificed at day 2 postinfection, and the brains were prepared as frozen sections. As analyzed by fluorescence microscopy, single eGFP-expressing cells were distributed in the parenchyma as a consequence of i.c. inoculation and the use of VRP that cannot propagate to other cells (Fig. 1). After costaining of the frozen sections for the marker proteins NeuN (neurons; left panel), GFAP (astrocytes; middle panel), and Mac-1a (microglia cells; right panel), double-stained cells in overlays were unequivocally identified as neurons (Fig. 1, left panel). Cells positive for GFAP, as well as Mac-1a-positive cells, were negative for eGFP expression (Fig. 1, middle and right panels).

These data demonstrated clearly that neurons are the major target cells for VRP infection in the brain and are consistent with studies performed with wild-type VEE which also have defined neurons as the primary target cells for the virus (11, 21, 22).

VRP replicate in the brains of inoculated mice and cause encephalitis-like symptoms. To monitor VRP RNA replication in the CNS of i.c. inoculated mice, we isolated total RNA from the brains of mice which were infected with 2×10^6 IU of FLAG-PABP VRP for 6, 24, 48, and 96 h and performed quantitative real-time PCR on the viral plus- and minus-strand RNA. Positive- and negative-strand RNA species showed peaks at 24 and 48 h postinfection (hpi), respectively, and then dropped about 100-fold by 96 h, when fewer than 100 copies of transcripts were detectable (Fig. 2A).

These findings are consistent with the development of disease signs in the infected animals. VRP-infected mice started losing weight the day after inoculation, with loss of up to 25% of the starting body weight on days 2 and 3 after infection (Fig. 2B). During this time, the infected animals showed mild signs

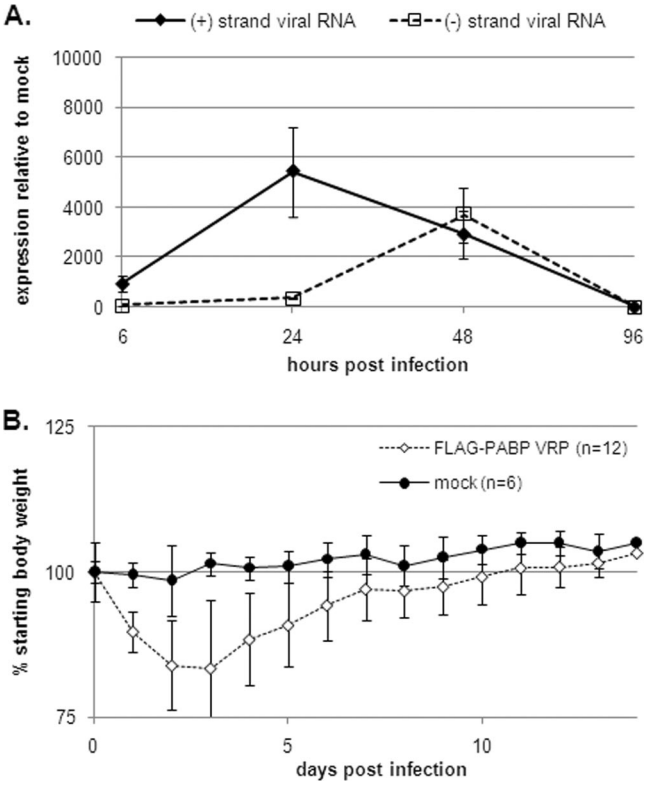

FIG. 2. VRP RNA replication in the brain and disease development in infected mice. (A) At 6, 12, 48, and 96 h after i.c. inoculation with 2×10^6 IU FLAG-PABP VRP, mice were euthanized, and after perfusion their brains were harvested for total RNA isolation. Viral positive- and negative-strand RNAs were quantified by real-time RT-PCR. The expression data presented are the means ± the standard errors of the means of four mice per group and are representative of two independent experiments. (B) Six- to 8-week-old female BALB/c mice were inoculated i.c. with 2×10^6 IU FLAG-PABP VRP. Control animals were inoculated with diluent alone. Animals were monitored for weight loss at 24-h intervals for 14 days. Each weight data point represents the arithmetic mean ± the standard deviation of 6 control (mock-inoculated) mice and 12 mice inoculated with FLAG-PABP VRP, and the results shown are representative of three independent experiments.

of disease such as ruffled fur, hunched back, and behavioral abnormalities, with 2 out of 12 infected mice showing tremors on day 3 postinfection. On day 4 postinfection, all of the infected mice started to recover and gain weight. Control animals, which were inoculated with diluent alone, showed no signs of disease or weight loss.

Taken together, these data indicate that inoculation of VRP directly into the brain can initiate a syndrome characterized by weight loss and mild signs of encephalitic-type disease. Active virus RNA replication, monitored by real-time PCR, was detectable until day 4 postinfection. This time course also was observed in eGFP expression studies, where eGFP-expressing cells were detectable from day 1 to day 4 postinfection, with only rare positive cells on day 7 postinfection (data not shown).

A robust proinflammatory cytokine response is induced early in infected and bystander cells following i.c. inoculation with VRP. Cytokine production by cells in infected tissue plays an important role in clearing a pathogen by facilitating accumulation and activation of the appropriate innate immune effectors. We focused our analysis on the key host defense gene that encodes beta interferon (IFN-β), whose antiviral function is especially important in VEE infection (28, 53, 61). Additionally, interleukin-6 (IL-6) and tumor necrosis factor alpha (TNF-α) were chosen because of their postulated contribution to BBB permeability changes and their proinflammatory immune functions (1, 2, 24).

The mRNP tagging method revealed an early and strong induction of mRNA for IFN-β (Fig. 3A) in infected cells. Indeed, IFN-β mRNA increased by 100-fold, became maximal at 12 hpi, and began to decline at 24 hpi. Analysis of cytokine expression in the total cell population of the infected brain showed that IFN-β expression was detectable at 6 hpi, became maximal at 12 hpi (~1,000-fold increase), and started to wane by 24 hpi. The induction of mRNA for IL-6 (Fig. 3B) in both the infected and total cell populations was also elevated within the first 6 h of infection and reached maximal increases of 500- to 7,000-fold at 12 to 24 hpi. TNF-α mRNA (Fig. 3C) expression was induced 10-fold in infected cells after the first 6 h of infection and was still increasing by 24 hpi. In the whole brain, TNF-α mRNA expression levels were detectable at 6 and 12 hpi at approximately 10-fold induction, which then increased to 2,000-fold at 24 hpi. From these data, we can conclude that the infected cells activate the surrounding cells, most likely microglia cells, to upregulate TNF-α expression. These findings predicted breakdown of the BBB, as well as upregulation of several leukocyte attractant chemokines in the infected brain.

VRP inoculation into the brain induces breakdown of the BBB and intercellular adhesion molecule 1 (ICAM-1) expression in the brain. Studies of models of autoimmunity and virus-induced neuroinflammation have provided evidence linking enhanced BBB permeability with the development of a CNS inflammatory response (15, 26, 59). To directly evaluate BBB integrity in VRP infection, we inoculated mice i.c. with 2×10^6 IU FLAG-PABP VRP and assayed for BBB permeability at 24, 48, and 96 h. One hour before their brains were harvested, mice were challenged with Evans blue, a dye normally excluded from the CNS. The results showed an increase in BBB permeability as early as 24 h after i.c. inoculation of FLAG-PABP VRP. The peak of permeability was reached at day 2 postinfection, and by day 4 postinfection the BBB showed no detectable signs of permeability. Control animals that received diluent i.c. showed no compromise of the BBB (Fig. 4A). The inoculation of FLAG-PABP VRP into the left rear footpad had no impact on the integrity of the BBB at any of the observed time points (Fig. 4B), and previous experiments showed by quantitative real-time PCR that no VRP reached the brain under these conditions (data not shown). A control i.c. injection of a null VRP construct (Fig. 4C) or an i.p. injection of 50 μg of poly(I:C) (Fig. 4B) resulted in levels of BBB permeability at 24 hpi comparable to those observed with FLAG-PABP VRP (Fig. 4A). UV treatment of FLAG-PABP VRP diminished the observed effect on BBB leakiness after i.c. inoculation, suggesting that the opening of the BBB is due to active viral RNA replication (Fig. 4D).

ICAM-1 plays an important role in intercellular interactions during inflammation and immunity (39). ICAM-1 is expressed constitutively on the vascular endothelium of the BBB, but its expression is generally low and inducible by TNF-α, IL-1β, and

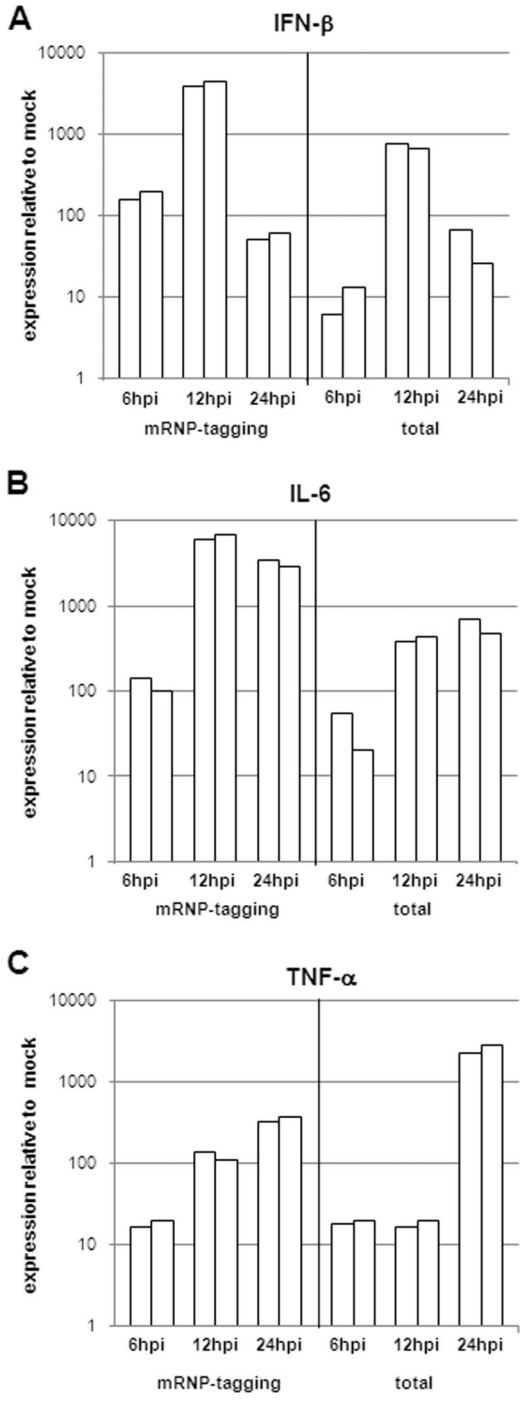

FIG. 3. A robust proinflammatory cytokine response is induced early in infected cells and bystander cells. Adult female BALB/c mice were anesthetized with a ketamine-xylazine anesthetic mixture and then inoculated i.c. with 2×10^6 IU of FLAG-PABP VRP. Mock-treated animals were inoculated with diluent alone. At 6, 12, and 24 h following infection, mice were euthanized and perfused with 1× PBS; their brains were then removed by dissection. Cellular RNA was isolated from mock-infected and VRP-infected mouse brains either by immunoprecipitation (mRNP tagging) or with an RNeasy Lipid Tissue Mini kit (total). cDNA was generated from each RNA preparation and assessed for changes in (A) IFN-β, (B) IL-6, and (C) TNF-α expression by real-time PCR. Two independent samples were normalized to *GAPDH* values and analyzed in comparison to mock-infected tissue (each bar represents one sample).

IFN. In case of an opening of the BBB, ICAM-1 is responsible for the firm attachment of leukocytes via the integrin LFA-1 to the endothelium and is essential for the transendothelial migration of T lymphocytes (14). Quantification of ICAM-1 mRNA expression in the VRP-infected brain as a whole showed increased levels at 6 hpi and a peak at 48 hpi, a time when the BBB was opened to its maximum (Fig. 4E).

An inflammatory chemokine response is initiated in the whole brain during VRP infection. Chemokine production by the cells in the area of an infection plays an important role in clearing a pathogen by facilitating accumulation of the appropriate immune effector cells (43, 45). At 24 hpi, expression levels of mRNAs for Ccl2/MCP-1 (which attracts monocytes and T cells), Ccl5/RANTES (which attracts leukocytes), and Cxcl10/IP-10 (which attracts monocytes and T cells and promotes T-cell adhesion) in the brain as a whole were at their peak and declined from 48 hpi through 96 hpi (Fig. 5). Expression of mRNA for Ccl3/MIP-1α, which signals an acute inflammatory state, mediates recruitment and activation of polymorphonuclear leukocytes, and is mainly produced by blood-derived monocytes, was generally lower than that of the mRNAs for Ccl2/MCP-1, Ccl5/RANTES, and Cxcl10/IP-10. Ccl3/MIP-1α mRNA also reached maximal expression at 48 hpi (Fig. 5).

Taken together, these data show that both infected and uninfected cells of the brain rapidly contribute to a robust innate immune response, setting the brain into an antiviral and alerted state. The observed cytokine (Fig. 3) and chemokine (Fig. 5) expression profiles suggest that the infected CNS is creating an environment for a directed adaptive immune response.

VRP inoculation and VRP RNA replication induce infiltration of leukocytes into the infected brain and proliferation of brain-residing microglia cells. It was expected that an elevated proinflammatory response, together with increased BBB permeability, would promote immune cell infiltration into brain tissue (44, 45). To characterize the infiltrating leukocytes, we inoculated mice i.c. with 2×10^6 IU of FLAG-PABP VRP and harvested their brains at days 1, 2, 4, 7, 9, and 14 after injection. Infiltrating cells were then isolated over a Percoll gradient and characterized by flow cytometry (Fig. 6).

In the CNS, microglia cells represent the major immune cell population and are classified by their expression of the myeloid marker CD11b and the hematopoietic marker CD45. In the resting state, microglia cells can be distinguished by low-to-intermediate expression of CD45 ($CD45^{dim}$) versus high CD45 ($CD45^{high}$) expression of monocytes and leukocytes (17, 49, 51). To study microglia cells and infiltrating monocytes in VRP-inoculated brains, we gated viable cells for CD11b and CD11c surface expression. The $CD11b^+$ $CD11c^-$ cell population was further gated into $CD45^{dim}$- and $CD45^{high}$-expressing populations. In mock-infected brains, we primarily detected $CD11b^+$ $CD45^{dim}$ microglia cells (15 to 18% of the total isolated cells) along with a low percentage of $CD11b^+$ $CD45^{high}$ cells (0.5 to 0.8%). Both populations are normally found in the naïve perfused mouse brain (18). The analysis of MHC class II surface expression demonstrated that these cells were in an inactivated and resting state (51). At day 1 postinfection, first $CD11b^+$ $CD45^{high}$ blood monocytes were detectable, indicating the start of infiltration of cells into the brain from the

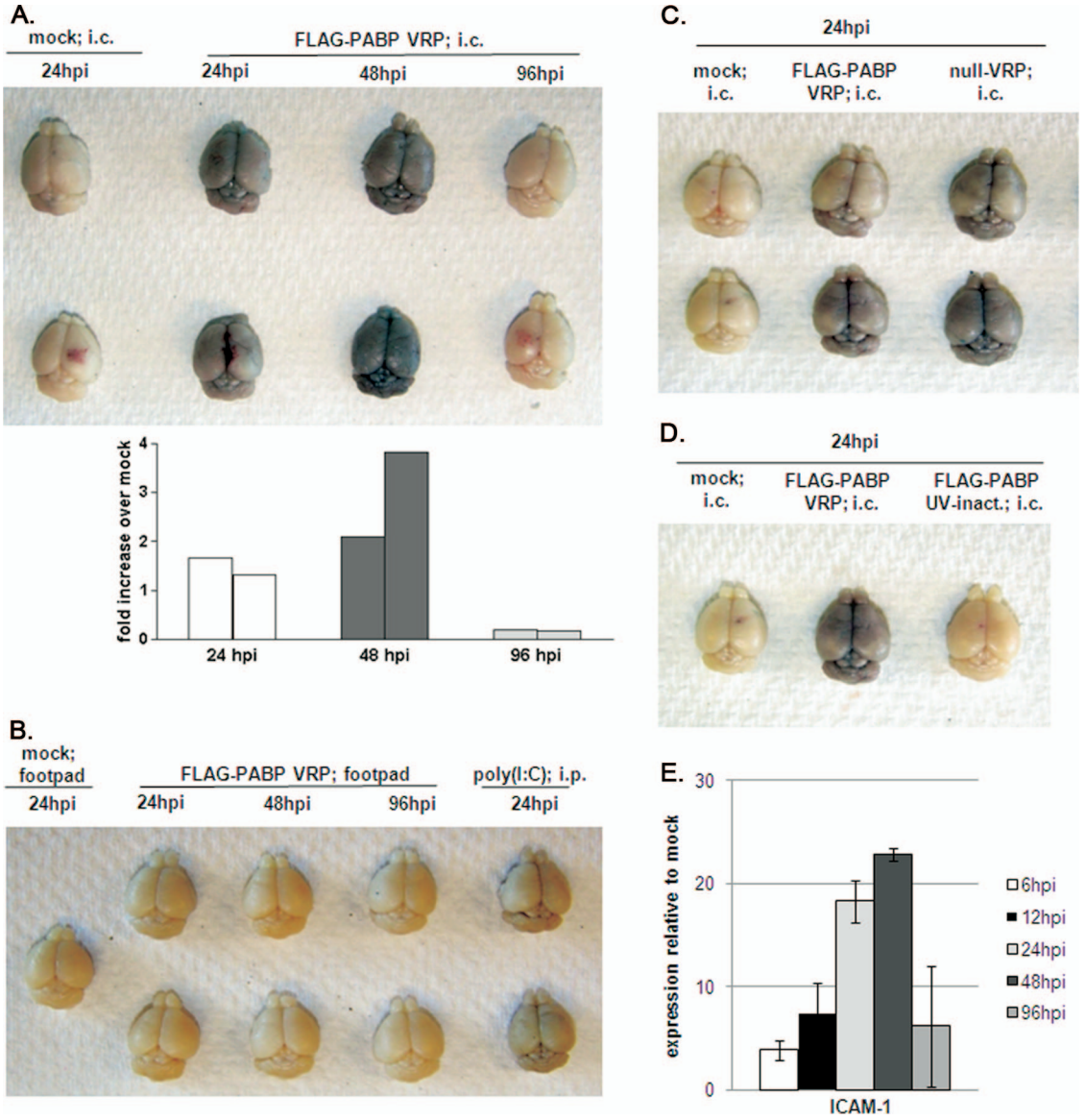

FIG. 4. VRP inoculation into the brain induces loss of BBB integrity, whereas the BBB remains intact after peripheral VRP inoculation. (A, top) Adult female BALB/c mice were anesthetized and then inoculated i.c. with 2×10^6 IU FLAG-PABP VRP or diluent alone. Their brains were harvested at 24, 48, and 96 h. One hour before their brains were harvested, mice were injected i.p. with 800 μl Evans blue dye. (A, bottom) Evans blue dye uptake in each brain sample shown in the upper panel is presented as the *n*-fold increase over that of mock-treated animals. Each bar represents an individual brain, with the left bar representing the upper brain and the right bar representing the lower brain. (B) Brains of mice inoculated in the left rear footpad with 2×10^6 IU FLAG-PABP VRP or diluent alone and harvested at 24, 48, and 96 h. Mice injected i.p. with 50 μg of poly(I:C) for 24 h served as a positive control. (C) Brains of mice treated as described for panel A but inoculated i.c. with diluent, 2×10^6 IU FLAG-PABP, or null VRP 24 h before their brains were harvested. (D) Brains of mice treated as described for panel A but inoculated with diluent alone, 2×10^6 IU FLAG-PABP VRP, or UV-inactivated FLAG-PABP VRP 24 h before their brains were harvested. (E) Expression levels of the gene for ICAM-1 determined by quantitative real-time PCR. The expression data presented are the means ± the standard errors of the means of four mice per group and are representative of two independent experiments.

periphery through the opened BBB. Also, proliferation of brain-residing microglia cells was first detectable, as indicated by increasing numbers of $CD11b^+$ $CD45^{dim}$ cells. Still, two distinct $CD45^{dim}$ and $CD45^{high}$ populations, representing brain-residing microglia cells and blood-borne monocytes, were distinguishable. Between day 2 and day 7 postinfection, increasing cell numbers were detectable in the inoculated brains. Residing microglia cells became activated, characterized by high CD45 surface expression, which made a distinction between microglia cells and infiltrating monocytes less clear at these times (17, 51). Both cell populations became highly activated, as indicated by upregulated surface expression of MHC class II. Former studies have shown that lymphocyte-derived IFN-γ has an important role in activating monocytes and microglia cells (31). In our gene expression studies, we were able to detect the expression of brain-derived IFN-γ starting at day 2 and day 4 postinfection (data not shown), i.e., the time point when T lymphocytes started to

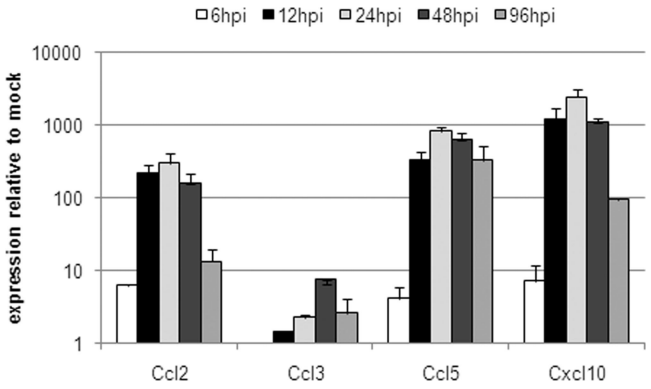

FIG. 5. Chemokine response in VRP-infected mouse brain. Groups of adult female BALB/c mice were anesthetized and then i.c. inoculated with 2×10^6 IU FLAG-PABP VRP or with diluent alone as a mock-infected control. At 6, 12, 24, 48, and 96 hpi, mice were euthanized and their brains were harvested for total RNA isolation. cDNA was synthesized, and expression levels of the genes for Ccl2/MCP-1, Ccl3/MIP-1α, Ccl5/RANTES, and Cxcl10/IP-10 were determined. The expression data presented are the means ± the standard errors of the means of four mice per group and are representative of two independent experiments.

infiltrate the brain. Starting at day 7 postinfection, the cell number was decreasing and the population of $CD11b^+$ $CD45^{dim}$ microglia cells started to reemerge. Between day 9 and day 14 postinfection, a reduction in the activation level of the remaining monocyte population was detectable, while the reestablished microglia cell population continued to be slightly activated.

Detectable in the uninfected brain were a small number of $CD4^+$ and $CD8^+$ T cells, as well as $B220^+$ B cells, with a presumed surveillance function (Fig. 7A) (44). By day 2 post infection a moderate influx of T and B lymphocytes was detectable. By day 4 postinfection, the infiltration of B lymphocytes was decreased while the influx of T lymphocytes, $CD4^+$ and $CD8^+$ cells, was increasing, establishing them as the major population of infiltrating lymphocytes in the infected brain. Since the BBB is closed by day 4 postinfection (Fig. 4A), increasing numbers of lymphocytes after this time are presumably due to induced proliferation in the brain. Over the period of observation, we detected a specific increase in $CD8^+$ T lymphocytes, which were also the dominant lymphocyte population at all of the time points analyzed (Fig. 7B). Interestingly, a significant portion of the $CD8^+$ T cells remained in the recovered brain at day 14 and the cell composition in the brains of infected animals at day 14 remained significantly different from that in mock-infected animals.

Microglia cells/monocytes and infiltrating leukocytes accumulate at sites of VRP-infected neurons. Fluorescence-activated cell sorter analysis revealed an early and strong infiltration of inflammatory leukocytes into the brain (Fig. 6 and 7), and studies with eGFP-VRP suggested that VRP infection was exclusively in neurons (Fig. 1). To localize the infiltrating cells in spatial relation to eGFP-VRP-infected neurons, additional immunofluorescence studies were performed.

Figure 8 shows a section 2 days post i.c. inoculation with eGFP-VRP in which $CD45^+$ cells localize predominantly in the vicinity of eGFP-positive cells in which VRP RNA is replicating. Mac-1a/CD11b-positive cells (data not shown) also were found predominantly in the vicinity of eGFP-expressing neurons, indicating a directed and specific accumulation of inflammatory microglia cells/monocytes and blood-borne leukocytes in infected CNS tissue (Fig. 8).

DISCUSSION

The molecular factors and pathways which initiate an innate immune response in the CNS at the earliest stages of a viral infection are largely unknown. These first, nonspecific mediators not only provide a first line of defense but also shape the adaptive immune response by attracting and activating immune cell populations and so contribute to the outcome of the infection.

In order to study the capability of resident brain cells to initiate a de novo innate immune response, we developed an approach enabling the examination of (i) the early host response to a VEE infection of neurons, (ii) the establishment of an initial proinflammatory network, and (iii) the first stages of an adaptive immune response in the CNS. Two techniques were previously established: the VRP system and the mRNP tagging system (29, 54). The VRP system substitutes single-cycle replicon particles for wild-type VEE, thus limiting viral replication to the first infected cells. This allowed modeling of the initial infection and communication between infected and uninfected cells without the confounding effects of viral spread through the CNS (11). The mRNP tagging system enables the isolation of host mRNA specifically from infected cells in vivo following VRP infection. The method facilitated a direct characterization of the host defense response specifically within the first infected cells, while simultaneous total RNA analysis allowed assessment of the collective response of both infected and uninfected cells in the entire brain in vivo. Konopka et al. (29) demonstrated a detectable antiviral response as early as 6 hpi in the draining lymph node of animals infected with VRP in the ipsilateral footpad. Further, this antiviral response acts in a paracrine manner by inducing a response in uninfected bystander cells in the lymph node. Taken together, these data demonstrated a biphasic innate immune response in the draining lymph node induced by VRP infection, as well as the power of the experimental system to study host gene expression in infected cells and their interaction with their uninfected environment (29).

In general, the main target cells for alphavirus infection in the CNS are neurons, but infection of astrocytes by VEE also has been described (10, 21, 50). To determine the target cell for VEE in the CNS, we inoculated eGFP-VRP i.c. into mice. By costaining brain-resident cells for specific cell markers, neurons appeared to be the dominant, if not exclusive, initial target cells for VRP; GFAP-positive cells and Mac-1a-expressing cells were negative for eGFP expression (Fig. 1). In terms of clinical signs of disease, weight loss, expression of eGFP, and detection of viral RNA by PCR, the infection peaked at day 2 and recovery appeared complete by day 7. While these experiments focused on the initial stages of CNS infection, it is evident that i.c. inoculation of VRP also will provide an interesting model for recovery from virus-induced encephalitis.

We then applied the VRP-mRNP tagging method to analyze the induction of proinflammatory cytokines in infected cells, as

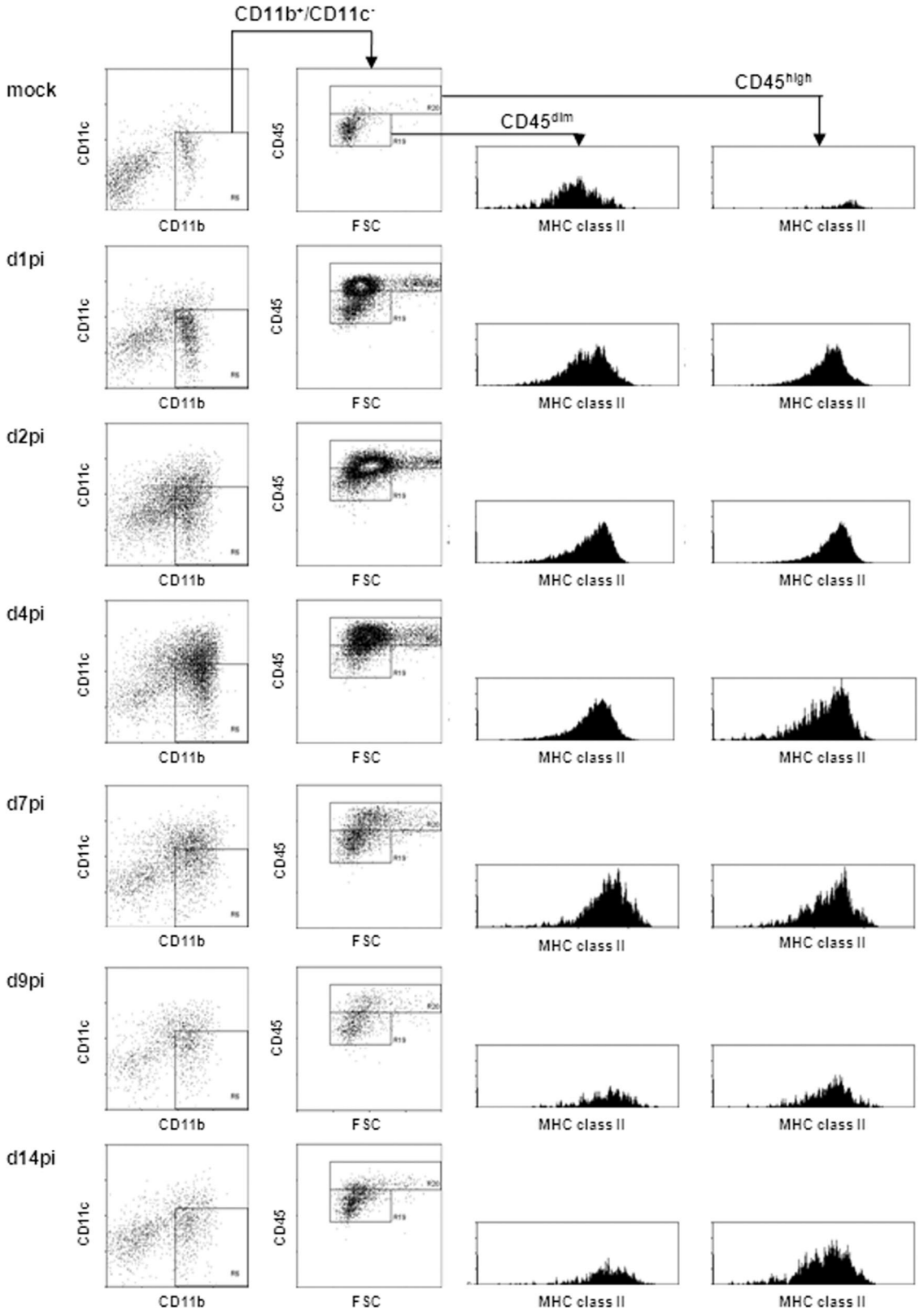

FIG. 6. VRP inoculation induces infiltration of activated monocytes into the infected brain and proliferation of brain-residing microglia cells. Adult female BALB/c mice were anesthetized and i.c. inoculated with 2×10^6 IU FLAG-PABP VRP. At days 1, 2, 4, 7, 9, and 14 postinfection, the brains of infected animals were harvested for isolation of infiltrating cells by Percoll gradient centrifugation. Viable cells were then characterized by determining cell surface markers by flow cytometry. Myeloid cells were identified by gating for $CD11b^+$ $CD11c^-$ cells. This gated cell population was then analyzed for CD45 surface expression and forward scatter (FSC) to distinguish brain-resident microglia cells ($CD11b^+$ $CD45^{dim}$) and blood-borne monocytes

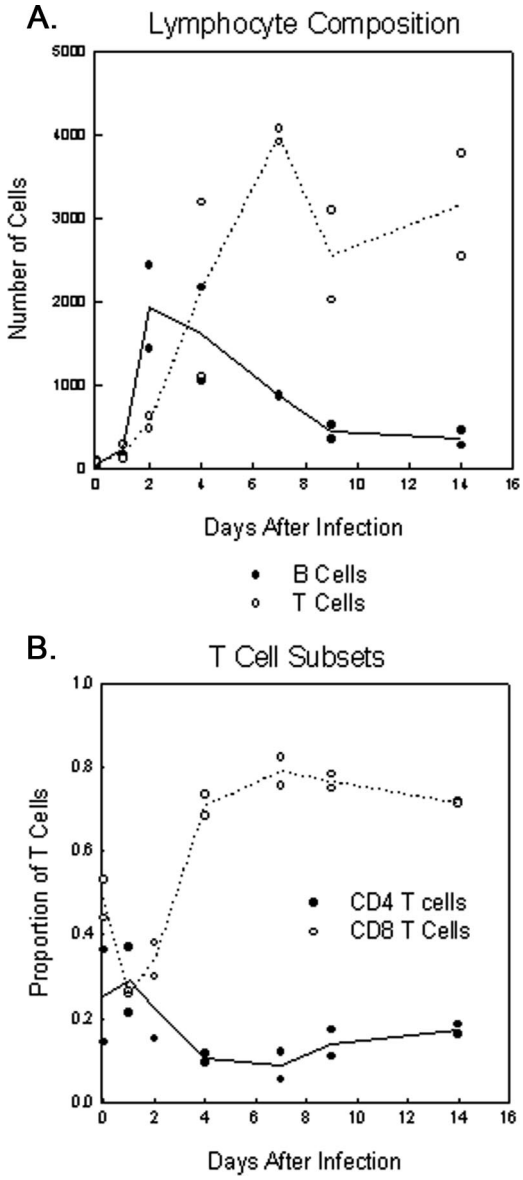

FIG. 7. VRP inoculation induces infiltration of $CD4^+$ and $CD8^+$ T lymphocytes. Adult female BALB/c mice were anesthetized and inoculated i.c. with 2×10^6 IU FLAG-PABP VRP or diluent alone as a mock-infected control. At days 1, 2, 4, 7, 9, and 14 postinfection, the brains of infected animals were harvested and infiltrating cells were isolated by Percoll density centrifugation. Cells were then characterized by determining cell surface markers by flow cytometry. To determine the total numbers of B lymphocytes and $CD4^+$ and $CD8^+$ T lymphocytes and the total number of recovered viable cells per brain per animal, cells were gated on CD11b and CD45 and then $CD45^+$ $CD11b^-$ cells were gated on B220 and CD3. $CD3^+$ $B220^-$ cells were then gated for CD4 and CD8. (A) Total lymphocyte composition and (B) the proportion of T-lymphocyte subsets at the indicated time points of infection are shown. Data shown for each time point are representative of two mice per group.

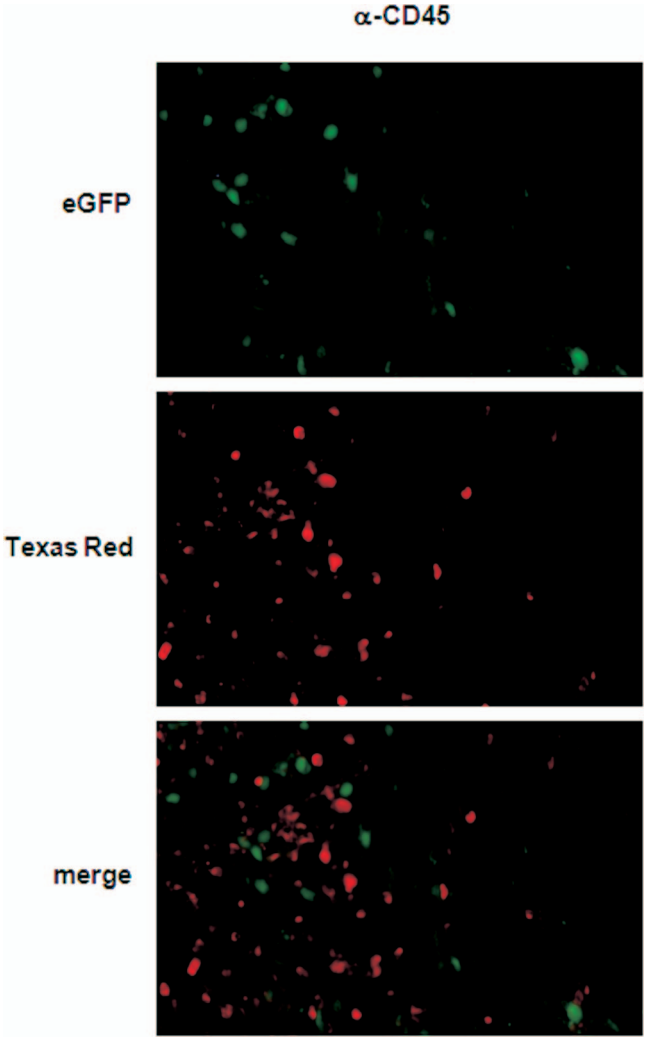

FIG. 8. Infiltrating leukocyte accumulation in VRP-inoculated mouse brains. Adult female BALB/c mice were inoculated i.c. with 2×10^6 IU eGFP-VRP or with diluent alone as a mock-infected control. At days 1, 2 (shown here), and 4 postinfection, mice were euthanized and perfused with 2% PFA. Their brains were then cryoprotected and sectioned at 10 μm. Infiltrating leukocytes were stained with an antibody specific for CD45 (middle panel), infected neurons were identified by eGFP expression (upper panel), and the overlay is shown in the bottom panel (magnification, ×200).

well as in uninfected bystander cells (Fig. 3) (29). We profiled gene expression in the infected neurons by the tagging method to measure the induction of IFN-β, IL-6, and TNF-α mRNAs. IFN-β is produced by virus-infected neurons in vitro and in vivo (13, 41) and is likely the most important antiviral cytokine (8, 34, 46). There was rapid and robust IFN-β expression in VRP-infected brain tissue in vivo (Fig. 3A). As VRP RNA

($CD11b^+$ $CD45^{high}$). Both populations ($CD11b^+$ $CD45^{dim}$ and $CD11b^+$ $CD45^{high}$) were further characterized for their activation status, indicated by their MHC class II surface expression level. (Left panel) Surface staining for CD11b and CD11c of cells isolated from the brain at 1, 2, 4, 7, 9, and 14 dpi, as well as a mock-infected control. (Middle panel) Surface staining for CD45 of $CD11b^+$ $CD11c^-$ cell populations. (Right panels) Surface staining for MHC class II of cells gated for intermediate (first panel) and high (second panel) levels of CD45 expression. Plots shown for each stain are representative of two mice per group. Three independent experiments gave similar results.

appeared to replicate exclusively in neurons, the increase in mRNA levels for these cytokines shown by the mRNP tagging method suggests that the source of the increased cytokine mRNA was infected neuronal cells. IFN-β mRNA expression reached maximal levels at 12 hpi and waned by 24 hpi. The IFN-β expression profile of total cells demonstrated kinetics similar to those of infected cells, but with lower expression levels. By using the tagging system, we were able to observe the CNS mounting a defense against the virus in both infected and uninfected cells. Gene expression profiles for IL-6 were similar to those for IFN-β, with strong and rapid expression by infected and uninfected cells at 6 hpi, increasing levels at 12 hpi, and maintained levels at 24 hpi (Fig. 3B). IL-6 has been described as an acute-phase protein with a variety of effects on the expression of other cytokines and mediators of inflammation (38). The data shown here indicate that infected and uninfected cells collectively initiate an alerted state in the entire brain. In the CNS, TNF-α is responsible for the activation of microglia cells and the induction of adhesion molecule expression by endothelial cells, thereby indirectly contributing to BBB permeability and the generalized expression of proinflammatory chemokines (32, 59). In this study, we found that TNF-α expression levels were increased over the analyzed period of time in the infected cells. Most striking, however, were the observed expression levels of TNF-α in bystander cells at 24 hpi, suggesting the development of significant neuroinflammation (Fig. 3C). Taken together, the data presented here show that (i) infected neurons are capable of expressing a wide range of inflammatory, immunomodulatory signals in vivo but also (ii) the power of the method to specifically analyze gene expression only in the small population of infected cells. This method provides an excellent tool for further study of not only the immunological response but also the neurological and other physiological functions of neurons in response to viral infection.

At the same time as the expression levels of TNF-α were at their peak, evaluation of the BBB showed compromised integrity (Fig. 4). Likewise, the mRNA expression levels of ICAM-1, which serves as an additional indicator of an open BBB, were also at their peak (Fig. 4E) (14). These results are consistent with the course of weight loss and disease symptoms of the infected mice after i.c. VRP inoculation (Fig. 2). At the time of high TNF-α expression and maximum permeability of the BBB (Fig. 3 and 4), the disease symptoms seemed to be most severe; animals started to recover by day 4 postinfection (Fig. 2), at the time when the BBB became closed again.

Several chemokines are expressed in the CNS and are thought to fulfill important functions in attracting both brain-residing microglia cells and blood-borne leukocytes to the site of insult and thereby shaping an appropriate adaptive immune response (4, 45). A gene expression analysis of proinflammatory chemokines revealed that the levels of Ccl2/MCP-1, Ccl5/RANTES, and Cxcl10/IP-10 were increased during the first 24 h of infection, with levels peaking at 24 to 48 hpi, at a time point when the BBB demonstrated the greatest permeability (Fig. 4 and 5). These chemokines are mostly secreted by activated microglia cells and attract mainly inflammatory monocytes and T lymphocytes (12, 19, 30). mRNA for Ccl3/MIP1-α, a chemokine usually expressed by blood-borne monocytes and not expressed by any brain-resident cells, first became detectable at low levels at 12 hpi and was detectable at somewhat higher levels at 48 hpi, suggesting that a minor population of activated blood-borne monocytes also invaded the brain (Fig. 5 and 6) (4, 45, 55).

Flow cytometry analysis revealed extensive infiltration of blood-borne leukocytes and proliferation of brain-resident microglia cells in the infected brain (Fig. 6 and 7), and accumulation of these cells around eGFP-positive neurons was detected by immunofluorescence (Fig. 8) (7, 40, 51, 59, 62). Early in the infection, increasing numbers of infiltrating monocytes and proliferating microglia cells were detectable, which showed an activated antigen-presenting phenotype, indicated by upregulated MHC class II expression, during the progression of the infection. Similar observations have been described previously for other models of viral neuroinfection like West Nile virus and mouse hepatitis virus or CNS autoimmune diseases like experimental autoimmune encephalomyelitis (7, 17, 40, 62). Starting at day 9 postinfection, reestablishment of a resting microglia cell population was detectable, which remained slightly positive for MHC class II expression. The observed levels of CNS-expressed chemokines mirrored the composition of the infiltrating cell population, as well as the times at which these cells appeared (Fig. 5 to 7). Infiltration of $CD4^+$ and $CD8^+$ T lymphocytes was detectable at day 2 postinfection, and over the analyzed time frame of 14 days, a consistent level of $CD8^+$ T cells was detectable (Fig. 7). An interesting aspect was the high number of mostly activated (MHC class II^{high}) immune cells that remained after the closing of the BBB.

Further investigation will examine (i) the characteristics of the possible switch from an inflammatory condition to an anti-inflammatory neuroprotective state, including the fate of infected neurons, and (ii) changes in the populations of immune cells that remain in the brain at later time points after clearing of the infection appears complete. Among the issues still to be examined are the mechanism by which the resting microglia cell population is reestablished, the effector function and fate of the $CD8^+$ T-cell population remaining after the closure of the BBB, the fate of infected neurons, and the mechanism of clearance and recovery.

Opening of the BBB may not only allow infiltration of cells from the circulation, but during infection, loss of BBB integrity also may allow a significant influx of virus. During the normal course of VEE infection initiated in the periphery, peak viremia is observed from 12 to 48 hpi, while the first replication of virus in the brain is detected at approximately 30 h (10, 21). This suggests that initial invasion of the brain from peripheral nerves, as suggested by Charles et al. (10), may trigger opening of the BBB and subsequent massive viral invasion from the blood. Such a scenario likely would require initial replication of virus in the brain, as peripheral infection with nonpropagating VRP did not cause opening of the BBB (Fig. 4) although significant cytokine mRNA induction was observed under these conditions (data not shown).

By using the VRP-adapted mRNP tagging method, we were able to specifically characterize the host defense response within the first cells infected with VEE, while simultaneous total RNA analysis allowed assessment of the collective response of both the infected and uninfected cell populations. That assessment demonstrated that the early innate immune response to VRP infection in the CNS was able to initiate an

adaptive immune response with a specific and directed infiltration and accumulation of immune effector cells in the vicinity of the infected neurons.

The studies performed here suggest that VRP directly injected into the brain are a powerful tool to model the de novo infection of neurons in a naïve CNS, to study the intrinsic capability of the CNS to initiate an appropriate innate immune response, and to examine the resolution of the infection. The model has unequivocally identified neurons as the major target of VEE infection in the CNS, has begun to elucidate the pattern of intercellular cytokine and chemokine signaling in infected and bystander cells, has revealed the opening of the BBB during infection, has demonstrated the specific infiltration of cells of the adaptive immune response during infection, and has shown clearance of the infection. Further refinement of the model will allow detailed elucidation of the innate and adaptive immune responses to VEE-induced encephalitis, infection of the brain in animals first exposed to peripheral VRP infection, and the virology of the disease.

ACKNOWLEDGMENTS

This research was supported by NIH SERCEB (Southeastern Regional Center of Excellence for Biodefense and Emerging Diseases) grant 3-U54 AI 057157-06S.

We thank members of the Carolina Vaccine Institute for helpful scientific discussions. We thank Martha Collier for generating and safety testing VRP used in this study. We thank Nancy Davis for critical reading of the manuscript. We also thank Janice Weaver at the LCCC/DLAM UNC histopathology core facility and Robert Bagnell and Victoria Madden at the UNC microscopy services laboratory.

REFERENCES

1. **Abbott, N. J., L. Rönnbäck, and E. Hansson.** 2006. Astrocyte-endothelial interactions at the blood-brain barrier. Nat. Rev. Neurosci. **7:**41–53.
2. **Allan, S. M., and N. J. Rothwell.** 2001. Cytokines and neurodegeneration. Nat. Rev. Neurosci. **2:**734–744.
3. **Aloisi, F.** 2001. Immune function of microglia. Glia **36:**165–179.
4. **Ambrosini, E., and F. Aloisi.** 2004. Chemokines and glial cells: a complex network in the central nervous system. Neurochem. Res. **29:**1017–1038.
5. **Aronson, J. F., F. B. Grieder, N. L. Davis, P. C. Charles, T. Knott, K. Brown, and R. E. Johnston.** 2000. A single-site mutant and revertants arising in vivo define early steps in the pathogenesis of Venezuelan equine encephalitis virus. Virology **270:**111–123.
6. **Bergmann, C. C., T. E. Lane, and S. A. Stohlman.** 2006. Coronavirus infection of the central nervous system: host-virus stand-off. Nat. Rev. Microbiol. **4:**121–132.
7. **Bréhin, A.-C., J. Mouriès, M.-P. Frenkiel, G. Dadaglio, P. Desprès, M. Lafon, and T. Couderc.** 2008. Dynamics of immune cell recruitment during West Nile encephalitis and identification of a new $CD19^{+}B220^{-}BST\text{-}2^{+}$ leukocyte population. J. Immunol. **180:**6760–6767.
8. **Byrnes, A. P., J. E. Durbin, and D. E. Griffin.** 2000. Control of Sindbis virus infection by antibody in interferon-deficient mice. J. Virol. **74:**3905–3908.
9. **Carson, M. J., J. M. Doose, B. Melchior, C. D. Schmid, and C. C. Ploix.** 2006. CNS immune privilege: hiding in plain sight. Immunol. Rev. **213:**48–65.
10. **Charles, P. C., E. Walters, F. Margolis, and R. E. Johnston.** 1995. Mechanism of neuroinvasion of Venezuelan equine encephalitis virus in the mouse. Virology **208:**662–671.
11. **Charles, P. C., J. Trgovcich, N. L. Davis, and R. E. Johnston.** 2001. Immunopathogenesis and immune modulation of Venezuelan equine encephalitis virus-induced disease in the mouse. Virology **284:**190–202.
12. **Chen, B. P., W. A. Kuziel, and T. E. Lane.** 2001. Lack of CCR2 results in increased mortality and impaired leukocyte activation and trafficking following infection of the central nervous system with a neurotropic coronavirus. J. Immunol. **167:**4585–4592.
13. **Delhaye, S., S. Paul, G. Blakqori, M. Minet, F. Weber, P. Staeheli, and T. Michiels.** 2006. Neurons produce type I interferon during viral encephalitis. Proc. Natl. Acad. Sci. USA **103:**7835–7840.
14. **Dietrich, J. B.** 2002. The adhesion molecule ICAM-1 and its regulation in relation with the blood-brain barrier. J. Neuroimmunol. **128:**58–68.
15. **Fabis, M. J., G. S. Scott, R. B. Kean, H. Koprowski, and D. C. Hooper.** 2007. Loss of blood-brain barrier integrity in the spinal cord is common to experimental allergic encephalomyelitis in knock out mice models. Proc. Natl. Acad. Sci. USA **104:**5656–5661.
16. **Fabry, Z., C. S. Raine, and M. N. Hart.** 1994. Nervous tissue as an immune compartment: the dialect of the immune response in the CNS. Immunol. Today **15:**218–224.
17. **Fischer, H. G., and G. Reichmann.** 2001. Brain dendritic cells and macrophages/microglia in central nervous system inflammation. J. Immunol. **166:** 2717–2726.
18. **Ford, A. A. L. Goodsall, W. F. Hickey, and J. D. Sedgwick.** 1995. Normal adult ramified microglia separated from other central nervous system macrophages by flow cytometric sorting. J. Immunol. **154:**4309–4321.
19. **Glass, W. G., M. J. Hickey, J. L. Hardison, M. T. Liu, J. E. Manning, and T. E. Lane.** 2004. Antibody targeting of the CC chemokine ligand 5 results in diminished leukocyte infiltration into the central nervous system and reduced neurologic disease in a viral model of multiple sclerosis. J. Immunol. **172:**4018–4025.
20. **Gleiser, C. A., W. S. Gochenour, Jr., T. O. Berge, and W. D. Tigertt.** 1962. The comparative pathology of experimental Venezuelan equine encephalomyelitis infection in different animal hosts. J. Infect. Dis. **110:**80–97.
21. **Grieder, F. B., N. L. Davis, J. F. Aronson, P. C. Charles, D. C. Sellon, K. Suzuki, and R. E. Johnston.** 1995. Specific restrictions in the progression of Venezuelan equine encephalitis virus-induced disease resulting from single amino acid changes in the glycoproteins. Virology **206:**994–1006.
22. **Grieder, F. B., B. K. Davis, X. D. Zhou, S. J. Chen, F. D. Finkelman, and W. C. Gause.** 1997. Kinetic of cytokine expression and regulation of host protection following infection with molecularly cloned Venezuelan equine encephalitis virus. Virology **233:**302–312.
23. **Griffin, D. E.** 2001. Alphaviruses, p. 917–962. *In* D. M. Knipe, B. N. Fields, and P. M. Howley (ed.), Fields virology, 4th ed. Lippincott Williams & Wilkins, Philadelphia, PA.
24. **Griffin, D. E.** 2003. Immune responses to RNA-virus infections of the CNS. Nat. Rev. Immunol. **3:**493–502.
25. **Hickey, W. F.** 2001. Basic principles of immunological surveillance of the normal central nervous system. Glia **36:**118–124.
26. **Hooper, D. C., G. S. Scott, A. Zborek, T. Mikheeva, R. B. Kean, H. Koprowski, and S. V. Spitsin.** 2000. Uric acid, a peroxynitrite scavenger, inhibits CNS inflammation, blood-CNS barrier permeability changes, and tissue damage in a mouse model of multiple sclerosis. FASEB J. **14:**691–698.
27. **Jackson, A. C., and J. P. Rossiter.** 1997. Apoptotic cell death is an important cause of neuronal injury in experimental Venezuelan equine encephalitis virus infection of mice. Acta Neuropathol. **93:**349–353.
28. **Jordan, G. W.** 1973. Interferon sensitivity of Venezuelan equine encephalomyelitis virus. Infect. Immun. **7:**911–917.
29. **Konopka, J. L., L. O. Penalva, J. M. Thompson, L. J. White, C. W. Beard, J. D. Keene, and R. E. Johnston.** 2007. A two-phase innate host response to alphavirus infection identified by mRNP-tagging in vivo. PLoS Pathog. **3:**e199.
30. **Liu, M. T., B. P. Chen, P. Oertel, M. J. Buchmeier, D. Armstrong, T. A. Hamilton, and T. E. Lane.** 2000. Cutting edge: the T cell chemoattractant IFN-inducible protein 10 is essential in host defense against viral-induced neurologic disease. J. Immunol. **165:**2327–2330.
31. **Malone, K. E., S. A. Stohlman, C. Ramakrishna, W. Macklin, and C. C. Bergmann.** 2008. Induction of class I antigen processing components in oligodendroglia and microglia during viral encephalomyelitis. Glia **56:**426–435.
32. **Mayhan, W. G.** 2002. Cellular mechanism by which tumor necrosis factor-alpha produces disruption of the blood-brain barrier. Brain Res. **927:**144–152.
33. **Morrison, T. E., A. C. Whitmore, R. S. Shabman, B. A. Lidbury, S. Mahalingam, and M. T. Heise.** 2006. Characterization of Ross River virus tropism and virus-induced inflammation in a mouse model of viral arthritis and myositis. J. Virol. **80:**737–749.
34. **Müller, U., U. Steinhoff, L. F. Reis, S. Hemmi, J. Pavlovic, R. M. Zinkernagl, and M. Aguet.** 1994. Functional role of type I and type II interferons in antiviral defense. Science **264:**1918–1921.
35. **Neumann, H.** 2001. Control of glial immune function by neurons. Glia **36:**191–199.
36. **Niederkorn, J. Y.** 2006. See no evil, hear no evil, do no evil: the lessons of immune privilege. Nat. Immunol. **7:**354–359.
37. **Olson, J. K., and S. D. Miller.** 2004. Microglia initiate central nervous system innate and adaptive immune responses through multiple TLRs. J. Immunol. **173:**3916–3924.
38. **Perry, V. H., C. Cunningham, and C. Holmes.** 2007. Systemic infections and inflammation affect chronic neurodegeneration. Nat. Rev. Immunol. **7:**161–167.
39. **Phares, T. W., R. B. Kean, T. Mikheeva, and D. C. Hooper.** 2006. Regional differences in blood-brain barrier permeability changes and inflammation in the apathogenic clearance of virus from the central nervous system. J. Immunol. **176:**7666–7675.
40. **Ponomarev, E. D., L. P. Shriver, K. Maresz, and B. N. Dittel.** 2005. Microglial cell activation and proliferation precedes the onset of CNS autoimmunity. J. Neurosci. Res. **81:**374–389.
41. **Préhaud, C., F. Mégret, M. Lafage, and M. Lafon.** 2005. Virus infection

switches TLR-3-positive human neurons to become strong producers of beta interferon. J. Virol. **79:**12893–12904.
42. **Pushko, P., M. Parker, G. V. Ludwig, N. L. Davis, R. E. Johnston, and J. F. Smith.** 1997. Replicon-helper systems from attenuated Venezuelan equine encephalitis virus: expression of heterologous genes in vitro and immunization against heterologous pathogens in vivo. Virology **239:**389–401.
43. **Ransohoff, R. M., A. Glabinski, and M. Tani.** 1996. Chemokines in immune-mediated inflammation of the central nervous system. Cytokine Growth Factor Rev. **7:**35–46.
44. **Ransohoff, R. M., P. Kivisäkk, and G. Kidd.** 2003. Three or more routes for leukocyte migration into the central nervous system. Nat. Rev. Immunol. **3:**569–581.
45. **Rebenko-Moll, N. M., L. Liu, A. Cardona, and R. M. Ransohoff.** 2006. Chemokines, mononuclear cells and the nervous system: heaven (or hell) is in the details. Curr. Opin. Immunol. **18:**683–689.
46. **Ryman, K., W. Klimstra, K. Nguyen, C. Biron, and R. E. Johnston.** 2000. Alpha/beta interferon protects adult mice from fatal Sindbis virus infection and is an important determinant of cell and tissue tropism. J. Virol. **74:**3366–3378.
47. **Ryzhikov, A. B., E. I. Ryabchikova, A. N. Sergeev, and N. V. Tkacheva.** 1995. Spread of Venezuelan equine encephalitis virus in mice olfactory tract. Arch. Virol. **140:**2243–2254.
48. **Samuel, M. A., and M. S. Diamond.** 2006. Pathogenesis of West Nile virus infection: a balance between virulence, innate and adaptive immunity, and viral evasion. J. Virol. **80:**9349–9360.
49. **Santambrogio, L., S. L. Belyanskaya, F. R. Fischer, B. Cipriani, C. F. Brosnan, P. Ricciardi-Castagnoli, L. J. Stern, J. L. Strominger, and R. Riese.** 2001. Developmental plasticity of CNS microglia. Proc. Natl. Acad. Sci. USA **98:**6295–6300.
50. **Schoneboom, B. A., M. J. Fultz, T. H. Miller, L. C. McKinney, and F. B. Grieder.** 1999. Astrocytes as targets for Venezuelan equine encephalitis virus infection. J. Neurovirol. **5:**342–354.
51. **Sedgwick, J. D., S. Schwender, H. Imrich, R. Dörries, G. W. Butcher, and V. terMeulen.** 1991. Isolation and direct characterization of resident microglial cells from the normal and inflamed central nervous system. Proc. Natl. Acad. Sci. USA **88:**7438–7442.
52. **Shrikant, P., and E. N. Beneveniste.** 1996. The central nervous system as an immunocompetent organ: role of glial cells in antigen presentation. J. Immunol. **157:**1819–1822.
53. **Spotts, D. R., R. M. Reich, M. A. Kalkhan, R. M. Kinney, and J. T. Roehrig.** 1998. Resistance to alpha/beta interferons correlates with the epizootic and virulence potential of Venezuelan equine encephalitis viruses and is determined by the 5′ noncoding region and glycoproteins. J. Virol. **72:**10286–10291.
54. **Tenenbaum, S. A., C. C. Carson, P. J. Lager, and J. D. Keeene.** 2000. Identifying mRNA subsets in messenger ribonucleoprotein complexes by using cDNA arrays. Proc. Natl. Acad. Sci. USA **97:**14085–14090.
55. **Trifilo, M. J., C. C. Bergmann, W. A. Kuziel, and T. E. Lane.** 2003. CC chemokine ligand 3 (CCL3) regulates $CD8^+$-T-cell effector function and migration following viral infection. J. Virol. **77:**4004–4014.
56. **Vogel, P., D. Abplanalp, W. Kell, M. S. Ibrahim, M. B. Downs, W. D. Pratt, and K. J. Davis.** 1996. Venezuelan equine encephalitis in BALB/c mice: kinetic analysis of central nervous infection following aerosol or subcutaneous inoculation. Arch. Pathol. Lab. Med. **120:**164–172.
57. **Wang, E., R. A. Bowen, G. Medina, A. M. Powers, W. Kang, L. M. Chandler, R. E. Shope, and S. C. Weaver.** 2001. Virulence and viremia characteristics of 1992 epizootic subtype IC Venezuelan equine encephalitis viruses and closely related enzootic subtype ID strains. Am. J. Trop. Med. Hyg. **65:**64–69.
58. **Wang, P., J. Dai, F. Bai, K.-F. Kong, S. J. Wong, R. R. Montgomery, J. A. Madri, and E. Fikrig.** 2008. Matrix metalloproteinase 9 facilitates West Nile virus entry into the brain. J. Virol. **82:**8978–8985.
59. **Wang, T., T. Town, L. Alexopoulou, J. F. Anderson, E. Fikrig, and R. A. Flavell.** 2004. Toll-like receptor 3 mediates West Nile virus entry into the brain causing lethal encephalitis. Nat. Med. **10:**1366–1373.
60. **Weaver, S. C., C. Ferro, R. Barrera, J. Boshell, and J.-C. Navarro.** 2004. Venezuelan equine encephalitis. Annu. Rev. Entomol. **49:**141–174.
61. **White, L. J., J.-G. Wang, N. L. Davis, and R. E. Johnston.** 2001. Role of alpha/beta interferon in Venezuelan equine encephalitis virus pathogenesis: effect of an attenuating mutation in the 5′ untranslated region. J. Virol. **75:**3706–3718.
62. **Zhou, J., N. W. Marten, C. C. Bergmann, W. B. Macklin, D. R. Hinton, and S. A. Stohlman.** 2005. Expression of matrix metalloproteinases and their tissue inhibitor during viral encephalitis. J. Virol. **79:**4764–4773.